LETTERS

A laboratory demonstration of the capability to image an Earth-like extrasolar planet

John T. Trauger[1] & Wesley A. Traub[1]

The detection and characterization of an Earth-like planet orbiting a nearby star requires a telescope with an extraordinarily large contrast at small angular separations. At visible wavelengths, an Earth-like planet would be 1×10^{-10} times fainter than the star at angular separations of typically 0.1 arcsecond or less[1,2]. There are several proposed space telescope systems that could, in principle, achieve this[3–6]. Here we report a laboratory experiment that reaches these limits. We have suppressed the diffracted and scattered light near a star-like source to a level of 6×10^{-10} times the peak intensity in individual coronagraph images. In a series of such images, together with simple image processing, we have effectively reduced this to a residual noise level of about 0.1×10^{-10}. This demonstrates that a coronagraphic telescope in space could detect and spectroscopically characterize nearby exoplanetary systems, with the sensitivity to image an 'Earth-twin' orbiting a nearby star.

Coronagraphs are not new to astronomy[7], but only recently has the concept been extended to the imaging of Earth-like extrasolar planets (exoplanets) from space[8]. In space, free of the blurring effects of atmospheric turbulence, a coronagraph must further suppress light diffracted from the edges of the primary mirror (the well-known Airy rings[9]) as well as a surrounding field of speckles due to irregularities in the surface figure of the optics. If left uncontrolled, these effects spread starlight across the focal plane, completely overwhelming any faint planet image. The scattered light in a high-quality optical telescope in space (for example, the Hubble Space Telescope, HST) at a typically close angular separation of $4\lambda/D$ is about 10^{-3} times the peak intensity of the central star (here λ is wavelength, and D is the diameter of the telescope primary mirror). This angular separation roughly corresponds to an Earth-twin, at maximum angular separation, orbiting a star 10 pc distant, as observed by a 4-m telescope at 500 nm wavelength. However, the scattered background is about 10^7 times greater than an Earth-twin; it must be suppressed to obtain a clean exoplanet signal.

In practice, diffracted light from the edges of the primary mirror can be removed by a variety of well-studied coronagraph configurations[10–16], each with its own specific characteristics and limitations, including efficiency, spectral bandwidth and complexity. The coronagraph can be combined with a telescope in a single spacecraft[3] to form a system that can be tested for end-to-end performance before launch. This is a significant advantage in cost, complexity and risk when compared to other actively studied mission concepts[4–6], which all require multiple spacecrafts orbiting in precisely constrained formations—a technology that cannot be validated on the ground and has yet to be proven in space. Here we demonstrate suppression of diffracted light with a Lyot-type coronagraph, and suppression of the speckle field with a wavefront sensing and control technique that is applicable to all coronagraph types.

Our laboratory apparatus, the High Contrast Imaging Testbed[17] (HCIT), is detailed in Supplementary Information, where we describe the optical elements, the concept of a band-limited Lyot coronagraph, the use of a precision deformable mirror (DM) to create a high-contrast dark field of view, a demonstration of the speckle nulling procedure that senses and corrects errors in the optical wavefront, and a discussion of spectral bandwidth. Enclosed in a space-like environment inside a vibration-isolated and thermally controlled vacuum chamber at room temperature, this system captures the essential optical features of a space coronagraph.

We report here the results of two experiments with the HCIT, namely, a 'snapshot' and a 'movie'. The snapshot experiment simulates a single exposure of a star and exoplanet system by a space coronagraph, allowing a view of a one-sided region near the star. The movie experiment simulates a series of snapshots taken as the space coronagraph is rotated about the line of sight to the star, thereby allowing a search for exoplanets in an annular region around the star.

In the snapshot experiment, the image of the star is centred on the coronagraph mask and the DM is commanded so as to minimize the speckle intensity in the target field of view. This experiment used a simulated star, but no simulated planet. By offsetting the star to a clear part of the mask, we record what a planet would look like (Fig. 1a). With the star centred, a dark target field appeared (Fig. 1b). If a simulated planet had been present in this D-shaped field, it would have appeared as a bright spot resembling Fig. 1a. Quantitatively, the data plotted in Fig. 1c show: curve A, the azimuth-averaged intensity of the star in the target field, without the focal plane mask present; curve B, the azimuth-averaged intensity of the star in the target field, with the focal plane mask, and with the DM set to minimize the average intensity in this field; and curve C the same as B except before DM correction. As shown in curve B, the average intensity is about 6×10^{-10} times the peak intensity of the star in a field between $4\lambda/D$ and $10\lambda/D$ on one side of the star. This snapshot experiment shows that the present apparatus, in a single exposure, is capable of suppressing both the diffracted and scattered light around a star, down to a contrast level that is slightly better than a Jupiter, but not quite as low as an Earth[18].

This experiment validates many, but not all, of the critical elements of an actively corrected space coronagraph for exoplanet imaging. It is a simple, stable coronagraph configuration, operating in a space-like environment, with contrast performance that can be accurately modelled end-to-end using the known characteristics of the optical elements. It illustrates a robust method of optical wavefront sensing and control that requires only the DM and a sensor in the focal plane to analyse the image of a star. It shows that current DMs are capable of suppressing scattered light to contrast levels and separations representative of a planet-finding mission and, as the movie experiment shows below, that the precision DM settings remain stable over periods of hours or more without feedback.

However, the experiment lacks a simulator for a large telescope structure in space. We briefly consider the flight system characteristics

[1]Jet Propulsion Laboratory, California Institute of Technology, 4800 Oak Grove Drive, Pasadena, California 91109, USA.

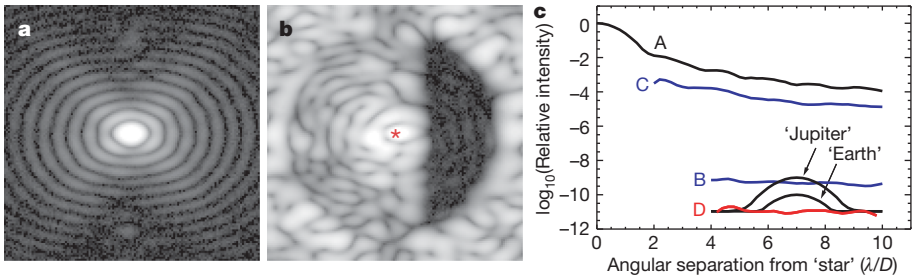

Figure 1 | Representative coronagraph images and intensity profiles. **a**, The appearance of a 'planet' offset from the star (and therefore not occulted by the coronagraph mask). The horizontal elongation of the diffraction rings is a result of the Lyot aperture (see Supplementary Information). **b**, The high-contrast coronagraph 'dark half-field' to the right of the masked central star (at the location of the red asterisk). **c**, Plots of relative intensity versus angular separation from the 'star'. Curve A, data from **a**; curve B, data from **b**; curve C, the coronagraph contrast before wavefront correction (with the DM nominally flat); curve D, the r.m.s. background obtained by roll deconvolution of a set of coronagraph images (obtained by subtracting the azimuthally averaged background in Fig. 2c). Intensity profiles for a nominal Earth and Jupiter in reflected starlight are included for reference. These are equal in intensity to the planets in Fig. 2, but centred at a separation of $7\lambda/D$ for clarity, and standing above the roll-deconvolved r.m.s. background. Images and intensity curves are displayed on logarithmic scales.

needed to carry this coronagraph concept forward to a viable space mission. System considerations will include our ability to manufacture an optical system to the required tolerances; our ability to make the necessary alignments and adjustments in orbit with demonstrated wavefront sensing and control methods; and our ability to maintain, within acceptable limits, critical alignments that may vary on timescales shorter than the wavefront sensing and control cycle (for example, less than 90 min). In Table 1, we list representative engineering tolerances for the most important sources of wavefront error in a 4-m telescope with a Lyot coronagraph.

The experiment was performed in polarized, narrowband laser light rather than unpolarized, continuum starlight filtered to a 10–20% ($\delta\lambda/\lambda$) bandwidth as would be required for photometric studies in astronomy. As we discuss further in Supplementary Information, our coronagraph is insensitive to polarization, working equally well in polarized and unpolarized light. We are currently addressing the question of spectral bandwidth in stages. Early experiments with 2% bandwidth yield a contrast of 1×10^{-9} using the same coronagraph masks and speckle nulling procedure as above (B. Kern, personal communication), and models indicate this can be improved to the contrast levels seen in narrowband light. Initial experiments with 10% bandwidth light, again with the same coronagraph mask and speckle nulling procedure, produced a contrast of 4×10^{-9}. Our model predicts that contrast with 10% bandwidth will be improved by about an order of magnitude using new coronagraph masks now being manufactured with standard techniques and common materials. This is an active area of development and a pathfinder for the ultimate space mission, as described in greater detail in Supplementary Information.

In the movie experiment, to simulate a coronagraph operating in space, we continuously repeated the snapshot experiment 480 times over a period of 5 h. The apparatus was very stable during this period; it was not adjusted in any way between exposures. The background speckle field evolved slowly, owing to room temperature changes and mechanical relaxation, much as might be expected in a coronagraph in space.

The movie experiment demonstrates the process of planet discovery with a space coronagraph, as follows. As shown in Fig. 2a, we hypothesize a space coronagraph that is aimed at a nearby star (centred behind the asterisk), with the background starlight suppressed in the target field, as in the snapshot experiment. We assume that the space coronagraph is rotated in small increments, so that the dark target field successively covers regions that ultimately fill the complete annular region between angular separations of $4\lambda/D$ and $10\lambda/D$ on the sky. For illustration, we show 12 discrete 30° steps in Fig. 2a, but in the computation we use 48 steps of 7.5° each, and in each step we co-add 10 sequential exposures, using a total of 480 exposures.

Lacking a simulated planet, we added attenuated copies of the star to each exposure, at the sky locations shown in Fig. 2a by the three coloured objects. This procedure is valid because we have previously shown that the presence of a planet in the speckle field of a star has no effect whatsoever on our wavefront correction algorithm[19]. The orbital positions were chosen artificially so that the projected planetary system could be captured in a single image here.

Table 1 | Critical engineering tolerances for a flight system

Significant sources of wavefront error	r.m.s. tolerance	Timescale	HST comparison
Precision of the DM settings*	0.014 nm*	>90 min	NA (no DM)
Telescope pointing jitter			
Body pointing of telescope (spacecraft momentum wheels)	35 mas	Active (0.1 Hz)	3–5 mas
Star on the coronagraph mask (fine steering mirror)	2.5 mas	Active (10 Hz)	NA (no FSM)
Surface of the primary mirror, by spatial scale across the PM			
$D/4$ and larger (specification, stability)	8 nm, 1.6 nm	Continuous	9 nm, unknown
$D/50$ to $D/4$ (polish and quilting artefacts, stability)	7 nm, 0.014 nm	>90 min	7 nm, similar
Particulate contamination (dust and micro-meteor pits)	Level 750	Years	Level 750 or better
Coating reflectance uniformity ($D/50$ to $D/4$)	0.25%	Years	Unknown
Surface quality of small optics (specification, stability)	1 nm, 0.014 nm*	>90 min	8 nm, similar
Telescope alignment (separation of the SM and PM)	1,000 nm	Continuous	2,000 nm

Representative engineering tolerances are shown for the dominant sources of wavefront error in a 4-m exoplanet imaging telescope with a Lyot coronagraph, and an HST comparison. The system architecture balances difficult requirements across the flight system, based on commercially available components and trades between competing engineering parameters, and a relaxation of optical tolerances using the DM for active wavefront correction. The tabulated numbers were derived by scaling from the (1.5-m) Eclipse[23] and TPF-C (8-m) SpeckleCam[22] engineering point designs. For the purpose of illustration, engineering tolerances are expressed in terms of their effect, δC, on the contrast metric C for the system overall. The cumulative effect of various independent sources of wavefront error can be approximated as the linear sum of their individual δC allocations, a computation that is equivalent to a quadratic sum of random, uncorrelated wavefront errors. With this understanding, each tolerance in the table has been scaled to contribute a δC no greater than about 1×10^{-11} (roughly one-tenth the brightness of an exo-Earth) to the overall contrast error budget. Some of these drift slowly over time and may be regarded as static errors, to be swept away with each new cycle of speckle nulling. Others, varying on shorter timescales, must be actively maintained within acceptable limits during the time between nulling cycles. In practice, a particular tolerance could be allocated a larger fraction of the overall contrast budget than shown here, but only at the expense of tighter requirements elsewhere in the system. Tolerances are presented along with expected timescales for significant variations (see Supplementary Information for further explanation of these tabulated values). NA, not applicable; FSM, fine steering mirror; PM, SM, telescope primary and secondary mirrors.
* Stability tolerances demonstrated in this Letter.

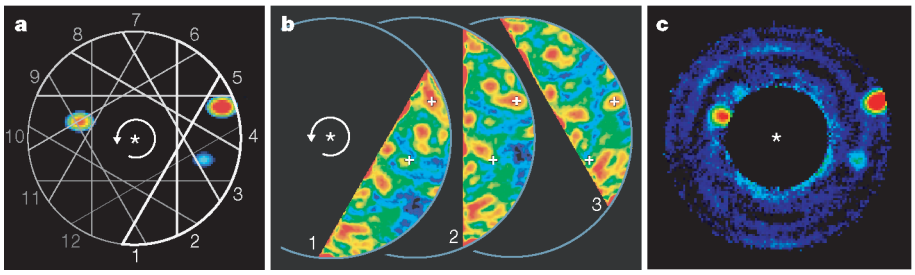

Figure 2 | Laboratory images demonstrate contrast at levels required to detect an Earth-twin. a, Three planet images are shown on the sky. The planets are copies of the measured star but reduced in intensity by factors of (10, 5 and 1) $\times 10^{-10}$, corresponding to the typical intensities of Jupiter, half-Jupiter and Earth, respectively. The Earth-twin is at about 4 o'clock, and the Jupiter-twin at 2 o'clock. The D-shaped field of view rotates on the sky as the spacecraft is rotated about the line of sight to the star (asterisk), as illustrated by the numbered segments drawn with successively fainter outlines as the rotation sequence progresses in time. **b**, Three sample images at different rotation angles illustrate the observing sequence. Note that the planets (white '+' signs) are fixed in inertial space, and just barely visible. The rotation sequence continues to fill a full annular field of view. **c**, Roll deconvolution is applied to the data, removing the background speckles that rotate with the spacecraft, and keeping the part of the image (planets) fixed in the sky (see also Fig. 1 for relative intensities). The planets stand out clearly against the residual background noise, which is the time-varying part of the speckles.

Three snapshots of the planets-plus-speckle field are shown in Fig. 2b. With a relative speckle intensity of about 6×10^{-10} in each snapshot, the planets (centred under the white '+' signs) are barely visible. This combination of a slowly evolving instrumental background that is fixed with the rotating spacecraft, plus an astronomical object that is fixed in inertial space, has been encountered before with images from the HST. The technique of removing the background speckle field while retaining the astronomical objects in the image[20,21] is known as 'roll deconvolution'. We applied a roll deconvolution algorithm to the present sequence of laboratory background plus superposed planet images (J. Krist, personal communication). The result is shown in Fig. 2c, where we see that all three planets stand out clearly. Further, subtracting the azimuthally averaged background field yields an r.m.s. uncertainty of about 0.1×10^{-10}, as indicated by curve D in Fig. 1c. The Earth and the Jupiter intensities are shown added to the background from roll-deconvolution, and superposed for clarity.

The movie experiment is an existence proof that it is possible to extract exoplanets close to a star, even when the residual speckle intensity is comparable to, or greater than, the planet intensities. We believe, however, that for planet detection and characterization a space coronagraph should be designed to even stricter standards, with roughly a factor of ten weaker speckles than achieved in the present experiments. The present work is a step towards this goal, but more work remains. Further laboratory work now in progress is focused on pushing the speckle background lower, broadening the spectral bandwidth, suppressing speckles simultaneously on both sides of the star with a pair of DMs[22], and increasing the radial field of view, both inward and outward. The present work lays the groundwork for the development of future missions[2,23] that will, for the first time, explore nearby Earth-like exoplanet systems by direct imaging and spectroscopy.

Received 28 September 2006; accepted 26 February 2007.

1. Des Marais, D. J. *et al.* Remote sensing of planetary properties and biosignatures on extrasolar terrestrial planets. *Astrobiology* **2**, 153–181 (2002).
2. Brown, R. A. Single-visit photometric and obscurational completeness. *Astrophys. J.* **624**, 1010–1024 (2005).
3. Traub, W. A. *et al.* TPF-C: status and recent progress. *Proc. SPIE* **6268**, OT1–OT14 (2006).
4. Kaltenegger, L. & Fridlund, M. The Darwin mission: search for extra-solar planets. *Adv. Space Res.* **36**, 1114–1122 (2005).
5. Henry, C. *et al.* Terrestrial Planet Finder: architecture, mission design, and technology development. *Proc. SPIE* **5491**, 265–274 (2004).
6. Cash, W. Detection of Earth-like planets around nearby stars using a petal-shaped occulter. *Nature* **442**, 51–53 (2006).
7. Lyot, B. A study of the solar corona and prominences without eclipses. *Mon. Not. R. Astron. Soc.* **99**, 580–594 (1939).
8. Guyon, O., Pluzhnik, E. A., Kuchner, M. J., Collins, B. & Ridgway, S. T. Theoretical limits on extrasolar terrestrial planet detection with coronagraphs. *Astrophys. J. Suppl.* **167**, 81–99 (2006).
9. Born, M. & Wolf, E. *Principles of Optics* (Cambridge Univ. Press, New York, 2002).
10. Kuchner, M. J. & Traub, W. A. A coronagraph with a band-limited mask for finding terrestrial planets. *Astrophys. J.* **570**, 900–908 (2002).
11. Kuchner, M. J., Crepp, J. & Ge, J. Eighth-order image masks for terrestrial planet finding. *Astrophys. J.* **628**, 466–473 (2005).
12. Guyon, O. Phase induced amplitude apodization of telescope pupils for extrasolar terrestrial planet imaging. *Astron. Astrophys.* **404**, 379–387 (2003).
13. Kasdin, N. J., Vanderbei, R. J., Littman, M. J. & Spergel, D. N. Optimal one-dimensional apodizations and shaped pupils for planet-finding coronography. *Appl. Opt.* **44**, 1117–1128 (2005).
14. Vanderbei, R. J., Kasdin, N. J. & Spergel, D. N. Checkerboard-mask coronagraphs for high-contrast imaging. *Astrophys. J.* **615**, 555–561 (2004).
15. Soummer, R. Apodized pupil Lyot coronagraphs for arbitrary telescope apertures. *Astrophys. J.* **618**, L161–L164 (2005).
16. Riaud, P., Boccaletti, A., Baudrand, J. & Rouan, D. The four quadrant phase mask coronagraph. *Publ. Astron. Soc. Pacif.* **115**, 712–719 (2003).
17. Trauger, J. T. *et al.* Coronagraph contrast demonstrations with the high-contrast imaging testbed. *Proc. SPIE* **5487**, 1330–1336 (2004).
18. Trauger, J., Kern, B. & Kuhnert, A. *TPF-C Technology Milestone #1 Report* (JPL Document D-35484, Jet Propulsion Laboratory, Pasadena, 2006).
19. Borde, P. J. & Traub, W. A. High-contrast imaging from space: nulling in a low-aberration regime. *Astrophys. J.* **638**, 488–498 (2006).
20. Heap, S. R. *et al.* Space Telescope Imaging Spectrograph coronagraphic observations of β-Pictoris. *Astrophys. J.* **539**, 435–444 (2000).
21. Lowrence, P. J. *et al.* An infrared coronagraphic survey for substellar companions. *Astron. J.* **130**, 1845–1861 (2005).
22. Krist, J., Trauger, J. & Moody, D. Studying a simple TPF-C. *Proc. SPIE* **6265**, 3O1–3O11 (2006).
23. Trauger, J. *et al.* The Eclipse Mission: a direct imaging survey of nearby planetary systems. *Proc. SPIE* **4854**, 116–128 (2002).

Supplementary Information is linked to the online version of the paper at www.nature.com/nature.

Acknowledgements The speckle nulling algorithm is due to C. Burrows. Development of the HCIT facility is an ongoing activity. Experiments were designed and simulated with the computational models of D. Moody. The HCIT control system was developed by B. Gordon and A. Niessner. Recent speckle nulling runs in white light have been carried out by B. Kern. The optical alignments were carried out by F. Shi and A. Kuhnert. The DM was manufactured by Xinetics Inc. The coronagraph mask was fabricated under the supervision of D. Wilson at JPL's Micro Devices Laboratory, on glass substrates supplied by Canyon Materials Inc. This work was carried out at JPL with the support of JPL and NASA.

Author Contributions J.T.T. performed HCIT experiments and data analysis at JPL; J.T.T. and W.A.T. co-wrote the paper.

Author Information Reprints and permissions information is available at www.nature.com/reprints. The authors declare no competing financial interests. Correspondence and requests for materials should be addressed to J.T.T. (john.trauger@jpl.nasa.gov).